NONLINEAR BUCKLING INSTABILITY ANALYSIS OF LONG-SPAN CABLE-STAYED BRIDGES UNDER DISPLACEMENT-DEPENDENT WIND LOAD

By Virote BOONYAPINYO*, Hitoshi YAMADA**, and Toshio MIYATA***

A finite-element approach to calculate a critical wind velocity for nonlinear flexural-torsional buckling instability of long-span cable-stayed bridges under displacement-dependent wind load is presented. An analytical modeling of buckling instability under wind load is formulated considering the three components of displacement-dependent wind load as well as geometric nonlinearity. A combination of the eigenvalue analysis and the updated wind-velocity bound algorithm is applied to automatically calculate the critical wind velocity. The results show that the incorporation of the three components of the displacement-dependent wind load as well as the geometric nonlinearity in the modeling of flexural-torsional buckling instability result in significant reduction of the critical wind velocity, compared with both the conventional linearized torsional divergence and linearized flexural-torsional buckling.

1. INTRODUCTION

The safety against buckling instability of a long-span cable-stay bridge under the displacement-dependent wind load, has recently become of great interest to bridge and structural engineers because as the bridge span increases, the bridge become more flexible and accordingly more susceptible to wind-induced problems. Under the effect of wind forces, the bridge is subjected to, and acts to resist, a drag force, a lift force and a pitching moment. These three components of wind forces are functions of wind angle of attack, in addition to wind velocity, and become rapidly larger as wind velocity increases, and then may result in one of two modes of static instability: torsional divergence and flexural-torsional buckling. The phenomenon of torsional divergence is characterized by a torsional instability, a monotonically increasing rotational to failure at a critical wind velocity at which the overturning pitching moment exceeds the elastic torsional resistance of the bridge structure. On the other hand, the flexural-torsional buckling is characterized by a combined vertical bending and torsional instability at a critical wind velocity at which the three components of the wind forces reduce the stiffness of the structure to zero.

* Graduate student, Dept. of Civil Engrg., Yokohama National University, Yokohama 240, Japan.

** Associate Professor, Dept. of Civil Engrg., Yokohama National University, Yokohama 240, Japan.

*** Professor, Dept. of Civil Engrg., Yokohama National University, Yokohama 240, Japan.

In addition, long-span cable-stayed bridges exhibit geometric nonlinearity due to : (1) combined effects of axial force and bending moment in the bridge deck and towers; (2) nonlinear behavior of cables caused by cable sag; and (3) bridge geometry change due to large displacements. All sources of this geometric nonlinearity should be considered in the nonlinear and instability analyses of this kind of bridge.

Three-dimensional nonlinear static analysis of cable-stayed bridge under bridge dead load have been studied by Nazmy and Ghaffarl [1], among others. Several investigators have recently studied the linearized flexural-torsional buckling of frame structures under displacement-independent load by finite element method [2-5]. Hirai et al. [6] have proposed the approximated formulas to estimate critical wind velocity for the flexural-torsional buckling of cable-supported bridges; however, the accuracy of this formula largely depends on the assumed mode of buckling. Previous researches on the static instability of cable-stayed bridges under wind load have generally been directed toward the linearized torsional divergence under the effect of pitching moment [7-8] or linearized flexural-torsional buckling under the effect of drag force. Very few researches, if any, have considered the nonlinear flexural-torsional buckling under the combined effects of the three components of displacement-dependent wind load.

In this paper, a finite-element approach to calculate the critical wind velocity for the nonlinear flexural-torsional buckling instability of long-span cable-stayed bridges under the three components of displacement-dependent wind load is presented. First, the nonlinear stiffness formulation of the bridge components is summarized, then the modeling of nonlinear flexural-torsional buckling instability is formulated. Next, a combination of the eigenvalue analysis and the updated wind-velocity bound algorithm is applied to automatically calculate the critical wind velocity. Finally, as a case study, the present method is applied to investigate buckling instability of a very long-span cable-stayed bridge with a center span length of 1000 meters. This bridge model was based on the design feasibility to represent the future trend in long-span cable-stayed bridges by Hoshino and Miyata [9].

2. NONLINEAR STIFFNESS FORMULATION OF BRIDGE COMPONENTS

2.1 Nonlinear Stiffness Formulation of Tower and Deck Elements

Tower and deck elements of a cable-stayed bridge are idealized by a beam-column element able to resist bending, shear, torsion, and axial forces. Large deformations that occur in these members under the combined effects of large bending moments and high axial forces produce a strong coupling between axial and flexural stiffness in these members. This coupling can be considered in the refined nonlinear analysis by introducing the concept of geometric stiffness matrix.

The element incremental equilibrium equation for a beam-column element in an updated Langrangian formulation is expressed as:

$$[k_e]\{u\} + [k_g^*]\{u\} = \{{}^2f\} - \{{}^1f\} \tag{1}$$

in which $[k_e]$ = the conventional linear elastic stiffness matrix of the element, $[k_g^*]$ = the (inconsistent) geometric stiffness matrix of the element, $\{u\}$ = the incremental displacement vector as shown in **Fig.1a**, $\{^2f\}$ = the element nodal external forces vector as shown in **Fig.1b** at the end of the incremental step, and $\{^1f\}$ = the element nodal internal forces vector as shown in **Fig.1b** at the beginning of the incremental step. The derivations of $[k_g^*]$ is given in detail in reference 10. The elements of $[k_g^*]$ are given in Appendix where (.) indicates a zero value and Wagner coefficient

$$\overline{K} = \frac{F_x I_p}{A} \; ; \quad (I_p = I_y + I_z) \tag{2}$$

In the preceding formulation the conventional rotational displacements (gradients of transverse displacements), is adopted. However, these displacement derivatives do not ensure continuity at angle joints when finite rotations of space structures are considered or when an out-of-plane buckling behavior of planar frames is concerned. Therefore, the Rodriguez's angles, which are commutative for finite rotations, is used to represent joint rotations, and yield, in addition to $[k_g^*]$, the joint correction matrix $[k_j]$: [5]

$$[k_j] = \frac{1}{2}\begin{bmatrix} 0 & M_z & -M_y \\ M_z & 0 & 0 \\ -M_y & 0 & 0 \end{bmatrix} \tag{3}$$

The $[k_j]$ is related only to the rotational degree-of-freedom and has the form for three-dimensional beam-column elements:

$$[k_j] = \mathrm{diag}\left[[0] \; [k_j^A] \; [0] \; [k_j^B] \right] \tag{4}$$

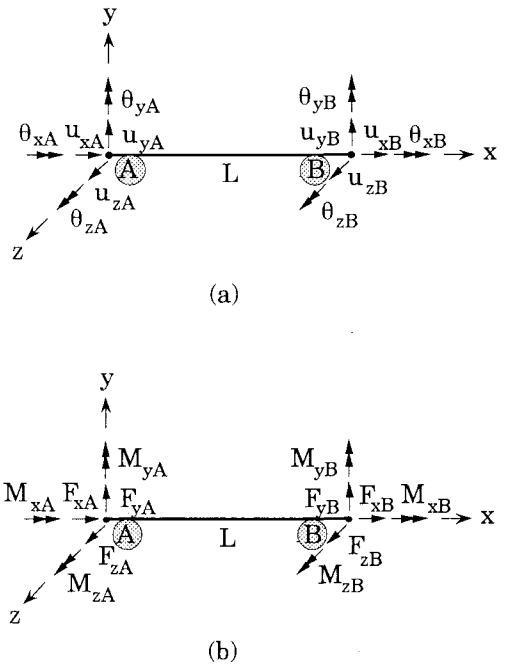

Fig.1 A beam-column element in local coordinate: (a) Degree of freedom; (b) Nodal forces

where [0] is the null 3 x 3 matrix and $[k_j^A]$ and $[k_j^B]$ are obtained from Eq. (3) by replacing (M_y, M_z) by $-(M_y, M_z)$ at nodes A and B, respectively.

Then, the element incremental equilibrium equation for a beam-column element in Eq. (1) is rewritten as:

$$[k_e]\{u\} + [k_g]\{u\} = \{^2f\} - \{^1f\}; \quad [k_g] = [k_g^*] + [k_j] \tag{5}$$

in which $[k_g]$ = the (consistent) geometric stiffness matrix for a beam-column element.

Therefore, the tangent stiffness matrix in local coordinates for beam-column elements is given by

$$[k_t] = [k_e] + [k_g] \tag{6}$$

It is interesting to note that due to the incorporation of the various nonlinear strains in an updated Lagrangian formulation, the geometric stiffness matrix in Eq. (5) can also be used to investigate instability of three-dimensional frame structures subjected to various forces, such as an axial force, a bending moment, a shear force, and a torsion. The validity of the present geometric stiffness matrix for buckling analysis is confirmed in the numerical test in reference 10.

2.2 Nonlinear Stiffness Formulation of Cable Elements

An apparent axial stiffness of a stay cable in a cable-stayed bridge is affected by the cable sag which is greatly influenced by the amount of tension in the cable. A convenient method to account for this effect in the cable axial stiffness is to replace the cable by a truss member with an equivalent modulus of elasticity for the cable. This concept was first introduced by Ernst and has been verified by several additional investigators. This equivalent cable modulus of elasticity is given by

$$E_{eq} = \frac{E}{1+\left[\frac{(wL)^2 AE}{12T^3}\right]} \tag{7}$$

in which E_{eq} = equivalent modulus of elasticity, E = cable material modulus of elasticity, w = weight per unit length of cable, L = horizontal projected length of the cable, A = cross section area of the cable, T = cable tension. Therefore, the elastic stiffness matrix in local coordinates for the cable element shown in Fig. 2 is given by:

$$[k_e] = \frac{AE_{eq}}{L_c}\begin{bmatrix} 1 & -1 \\ -1 & 1 \end{bmatrix} \tag{8}$$

where L_c = chord length of the cable.

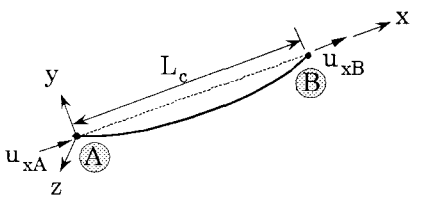

Fig.2 Degree of freedom of a cable element in local coordinate

In addition to elastic stiffness matrix, in a long-span cable-bridge bridge, the geometric stiffness matrix due to large nodal displacements of the stay cable should be considered because the concept of equivalent cable modulus of elasticity does not consider the change of geometry at cable ends. The geometric stiffness matrix of a three dimensional cable is simply equal to the geometric stiffness matrix of a three dimensional truss and is given by:

$$[k_g] = \frac{T}{L_c}\begin{bmatrix} [G] & -[G] \\ -[G] & [G] \end{bmatrix}; \quad [G] = \begin{bmatrix} 0 & 0 & 0 \\ 0 & 1 & 0 \\ 0 & 0 & 1 \end{bmatrix} \tag{9}$$

in which T is the axial force in the cable and is positive for a tension member.

Therefore, the tangent stiffness matrix in local coordinates for cable elements is given by

$$[k_t] = [k_e] + [k_g] \tag{10}$$

3. MODELING OF NONLINEAR BUCKLING INSTABILITY UNDER DISPLACEMENT-DEPENDENT WIND LOAD

In formulation of static instability under displacement-dependent wind load, the following loading assumption is made. The gravity loads (dead load, prestresses and some live load (if any)) are first applied and are kept constant, then the displacement-dependent wind load are simulated and applied on the bridge until the instability is reached.

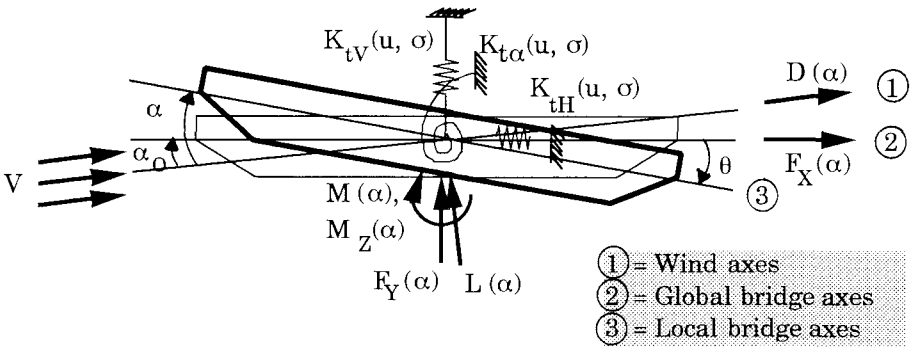

Fig.3 Motion of a bridge deck and three components of wind forces

Consider a section of bridge deck in a smooth oncoming flow, as shown in **Fig.3**, with static aerodynamic coefficients as a function of wind angle of attack shown in **Fig.4**. Assuming that under the effect of the mean wind velocity V with the angles of incidence α_0, the torsional displacement of deck is θ. Then the effective wind angles of attack is $\alpha = \alpha_0 + \theta$. The components of wind forces per unit span acting on the deformed deck can be written, with respect to wind axes, as

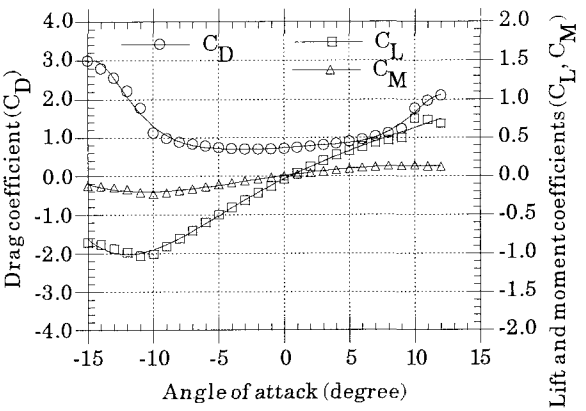

Fig.4 Static aerodynamic coefficients as a function of angle of attack [11]

$$D(\alpha) = \frac{1}{2}\rho V^2 A_n C_D(\alpha); \quad L(\alpha) = \frac{1}{2}\rho V^2 B C_L(\alpha); \quad M(\alpha) = \frac{1}{2}\rho V^2 B^2 C_M(\alpha) \tag{11 a-c}$$

where D, L, and M are mean drag force, lift force, and pitching moment per unit span shown in **Fig.3**, respectively; ρ is the air density; B is the deck width; A_n is the vertical projected area of deck; C_D, C_L, C_M are, respectively, drag, lift and pitching moment coefficients with respect to wind axes.

The projection of the wind forces in Eq. (11) on the global (undeformed) bridge axes shown in **Fig.3** are

$$F_X(\alpha) = D(\alpha)\cos(\alpha_0) - L(\alpha)\sin(\alpha_0); \quad F_Y(\alpha) = D(\alpha)\sin(\alpha_0) + L(\alpha)\cos(\alpha_0); \quad M_Z(\alpha) = M(\alpha) \tag{12 a-c}$$

These wind forces can be written in the alternative forms as

$$F_X(\alpha) = \frac{1}{2}\rho V_r^2 A_n C_X(\alpha); \quad F_Y(\alpha) = \frac{1}{2}\rho V_r^2 B C_Y(\alpha); \quad M_Z(\alpha) = \frac{1}{2}\rho V_r^2 B^2 C_Z(\alpha) \tag{13 a-c}$$

where

$$C_X(\alpha) = \left[C_D(\alpha) - C_L(\alpha)\tan\alpha_0\right]\sec\alpha_0; \quad C_Y(\alpha) = \left[C_L(\alpha) + C_D(\alpha)\tan\alpha_0\right]\sec\alpha_0;$$
$$C_Z(\alpha) = \left[C_M(\alpha)\right]\sec^2\alpha_0; \quad V_r = V\cos\alpha_0 \tag{14 a-d}$$

In Eqs. (13) and (14) V_r is relative wind velocity with respect to global bridge axes; $C_X(\alpha)$, $C_Y(\alpha)$ and $C_Z(\alpha)$ are the static aerodynamic coefficients with respect to global bridge axes.

The analytical modeling of nonlinear buckling under displacement-dependent wind load is composed of a two-step process as follows. In the first step process, analysis under initial wind forces of given wind velocity V with angle of incidence α_0 is performed in one step. The equilibrium equations is written as:

$$\left[K_e(u, \sigma) + K_g^G(u, \sigma)\right] U = \frac{1}{2}\rho V_r^2\left[A_n C_X(\alpha_0) + BC_Y(\alpha_0) + B^2 C_Z(\alpha_0)\right] \tag{15}$$

where K_e and K_g are found using both displacements u and stresses σ from gravity loads in the preceding analysis; V_r is given in Eq. (14d); $C_X(\alpha_0)$, $C_Y(\alpha_0)$ and $C_Z(\alpha_0)$ are, respectively, obtained from Eqs. (14 a-c) with $\alpha = \alpha_0$; superscript G means gravity loads.

In the second step process, nonlinear analysis under additional wind forces, induced by torsional deformation of the deck which in turn increases wind angle of attack, is performed as follows. After performing the above nonlinear analysis under initial wind forces, the total displacements and internal forces are obtained. From these displacements, the current static aerodynamic coefficients, C_D, C_L, C_M are computed and transformed to C_X, C_Y, C_Z. The linearized incremental equilibrium equations of the bridge subjected to additional wind forces for j^{th} step is written as

$$\left[K_e(u_{j-1}, \sigma_{j-1}) + K_g^{G+W}(u_{j-1}, \sigma_{j-1})\right]\Delta U_j$$
$$= \frac{1}{2}\rho V_r^2\left[A_n C_X(\alpha_j) + BC_Y(\alpha_j) + B^2 C_Z(\alpha_j)\right] - \frac{1}{2}\rho V_r^2\left[A_n C_X(\alpha_{j-1}) + BC_Y(\alpha_{j-1}) + B^2 C_Z(\alpha_{j-1})\right] \tag{16}$$

where superscript W stands for wind load. The above iterative process continues and at the end of each iterative cycle the additional wind forces are computed. The above process will converge for any given wind velocity less than the critical wind velocity. During iterative cycle, analysis of the tangent structure stiffness matrix make it possible to determine for each instance whether the equilibrium is stable, unstable or neutral.

The convergence criteria for given wind velocity reach when the Euclidean norm of static aerodynamic coefficients are less than the prescribed tolerance. The Euclidean norm is written as

$$\left[\sum_{j}^{N_a}\left\{C_k(\alpha_j) - C_k(\alpha_{j-1})\right\}^2 \Big/ \sum^{N_a}\left\{C_k(\alpha_{j-1})\right\}^2\right]^{1/2} \le \varepsilon_k, \quad k = X, Y, Z \tag{17}$$

in which ε_k represents prescribed tolerance, N_a= number of nodes subjected to displacement-dependent wind load.

It is interesting to note that due to the consideration of the three components of the displacement-dependent wind load in the analytical modeling, the safety against both the nonlinear flexural-torsional buckling instability and nonlinear torsional divergence can be investigated. If the effect of drag force D and lift force L are neglected in Eqs. (15) and (16), one obtains the analytical modeling of nonlinear torsional divergence. If the wind angle of incidence is zero, the wind axes coincide with global bridge axes, and then the wind forces F_X, F_Y and M_Z are, respectively, equal to D, L,and M.

4. CALCULATION OF CRITICAL WIND VELOCITY

Because the three components of wind loads acting on the bridge deck are nonlinear displacement-dependent wind load, the procedure for calculation of the critical wind velocity of cable-stayed bridge involves the outermost cycle of iteration, in addition to inner cycle of iteration for convergence of each given wind velocity described in the previous section. A combination of the eigenvalue analysis with respect to wind forces and the updated wind-velocity bound algorithm is applied to directly calculate the critical wind velocity instead of the trial-and-error method. The procedure can be summarized as follows.

Once the convergence of the three components of the displacement-dependent wind load of given wind velocity is reached (Eq. (17)), the eigenvalue analysis with respect to wind forces of given wind velocity is performed for predictor of the next wind velocity. The eigenvalue problem is expressed as

$$\left|\left(K_e + K_g^G\right) + \lambda K_g^W\right| = 0 \tag{18}$$

The eigenvalue in Eq. (18) should be modified to consider the derivative of the wind forces. Then the first approximation to the next chosen wind velocity is computed through method of equivalent drag force acting on the center span, and is given by

$$V_i^* = \sqrt{\frac{C_X\left(\alpha_{i-1}^{av}\right)}{C_X\left(\lambda_{i-1}\alpha_{i-1}^{av}\right)}\lambda_{i-1}}\ V_{i-1} = \sqrt{\lambda_{i-1}^*}\ V_{i-1} \tag{19}$$

where V_{i-1} = the wind velocity in the preceding outermost cycle of iteration; α_{i-1}^{av} = average torsional displacement of center span, obtained by using Simpson' s rule, in the preceding outermost cycle of iteration; λ_{i-1}^* = reduced buckling load factor. In Eq. (19) $C_X\left(\lambda_{i-1}\alpha_{i-1}^{av}\right)$ mean that C_X is computed using the average torsional displacements of deck time the buckling load factor λ in the preceding outermost cycle of iteration.

In addition, V_i^* in Eq. (19) should be satisfied the updated lower and upper wind-velocity bounds of the preceding outermost cycle of iteration, V_L and V_U, as follow:

$$V_L < V_i^* < V_U \tag{20}$$

When $V_i^* < V_L$, V_i^* is computed from Eq. (19) with $\lambda_{i-1}^* = 1 + 0.1\lambda_{i-1}$. When $V_i^* > V_U$, V_i^* is set to equal V_U.

Finally, since the wind forces become larger under increase in wind velocity and the structural stiffness is likely to decrease under the effect of wind forces, the final approximation to the next chosen wind velocity is modified into

$$V_i = \frac{V_{i-1} + V_i^*}{2} \tag{21}$$

where V_{i-1} = the wind velocity in the preceding outermost cycle of iteration.

When the preceding wind velocity is unstable, the next chosen wind velocity is computed from

$$V_i = \frac{V_{i-1} + V_L}{2} \tag{22}$$

It is clear that the processes of Eqs. (18)-(22) can be repeated for the search of the true critical wind velocity until the stable and unstable wind velocities close to each other. Typically, this procedure converges in a few outermost cycle of iteration. Flow chart for nonlinear static instability analysis under displacement-dependent wind load is shown in **Fig.5**.

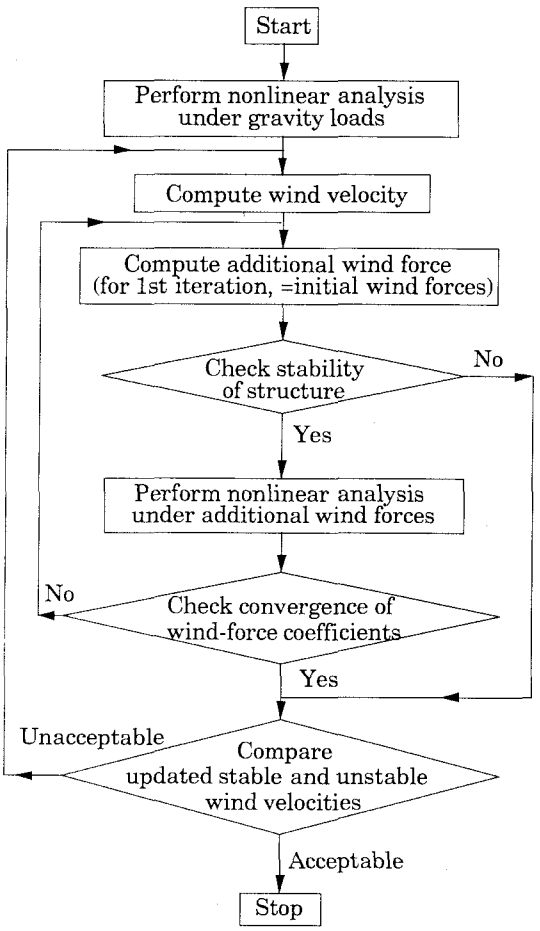

Fig.5 Flow chart for nonlinear static instability analysis under displacement-dependent wind load

5. NUMERICAL EXAMPLES

As a case study of the present method for calculation of the critical wind velocity for nonlinear flexural-torsional buckling instability under the three components of the displacement-dependent wind load, it is applied to a three-span continuous cable-stayed bridge with a 1000 meter center span and two 450 meter side spans. The general configuration of the bridge is shown in **Fig.6.** Longitudinal supports are all free except one hinge support at the left end of bridge deck, and lateral supports at the towers and deck ends are elastic. For the present purpose, the effects of auxiliary supports at side

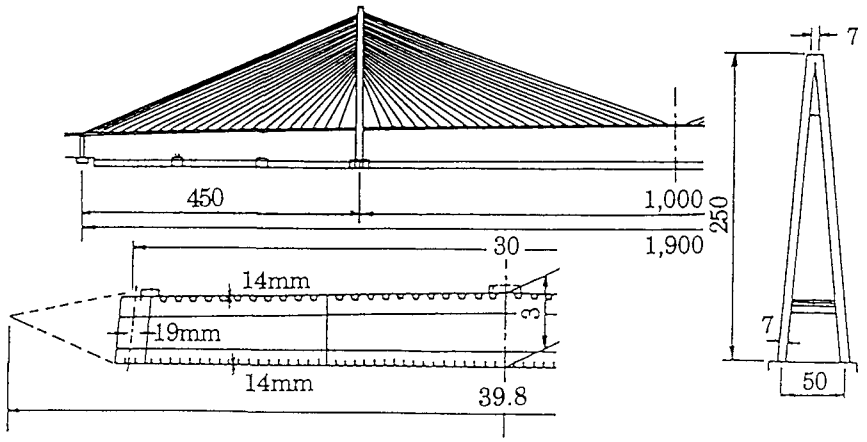

Fig.6 General configuration of the bridge with a three-span continuous deck studied (unit: m)

spans are not considered. The total dead load on the deck is equal to 26.5 t/m. The design wind velocity at 10 m height is 45 m/s and corresponding wind velocity at 56 m mean height of bridge deck is 57.15 m/s. In the following, the critical wind velocity will be referenced at deck elevation. The static aerodynamic coefficients for the bridge studied are assumed to coincide with **Fig.4** and are incorporated in computer program by using polynomial function representation. The three components of the nodal displacement-dependent wind load are considered for the deck while for the towers and cables only drag forces at initial wind angle of attack are considered. Based on the Honshu Shikoku Bridge Code [12], gust response in the longitudinal direction of bridge axis is taken into account in calculation of the drag force but neglecting in calculation of the lift force and the pitching moment. The convergence criteria for a given wind velocity is reached, when the Euclidean norm of the static aerodynamic coefficients, ε_X, ε_Y and ε_Z , are less than 5 %.

The three-dimensional finite element model for complete bridge used in this investigation is shown in **Fig.7**.

5.1 Nonlinear Flexural-Torsional Buckling Instability

The torsional behavior at mid-point of center span for linearized and nonlinear flexural-torsional buckling instability analysis is shown in **Fig.8**. As can be seen in the figure, the nonlinear buckling analysis under the three components of the displacement-dependent wind load results in significant reduction of the wind velocity, compared with the linearized buckling analysis under the initial wind forces. The critical wind velocity of 135 m/s obtained from the nonlinear buckling analysis is 55 % lower than that of 299 m/s obtained from the linearized buckling analysis. The corresponding buckling modes of linearized and nonlinear buckling analyses are shown in **Fig.9**. In the linearized buckling analysis, the phenomenon of asymmetric vertical bending and torsional models

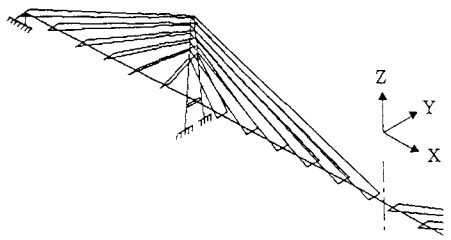

Fig.7 A three-dimensional finite element model

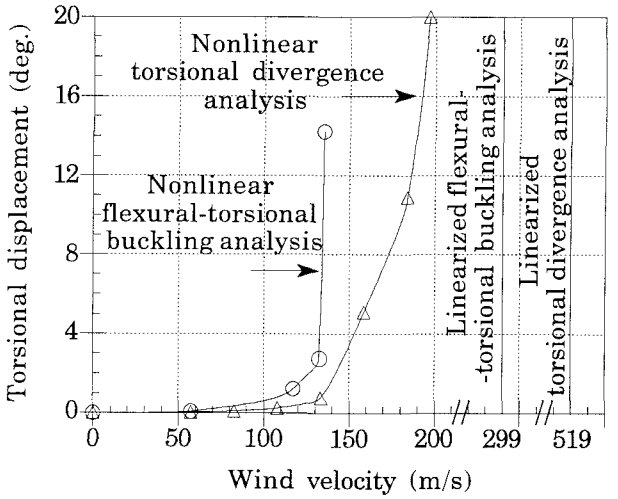

Fig.8 Torsional behavior at mid-point of center span for various instability analysis types

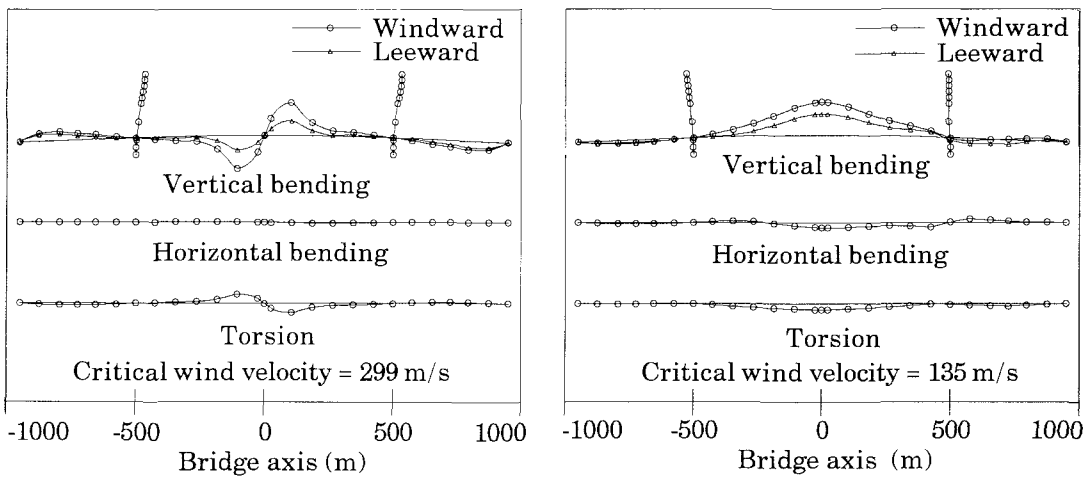

Fig.9 Buckling modes and corresponding critical wind velocities obtained from:
(a) linearized flexural-torsional buckling instability
(b) nonlinear flexural-torsional buckling instability

are probably due to: (1) the higher stiffness of upper cables which are back-anchored at side supports and (2) the effects of the geometric stiffness matrix of the tension cables [10]. However, in the nonlinear buckling analysis, the relaxation of the elastic stiffness of the upper cables in the center span probably leads to symmetric vertical bending and torsional modes. It should be noted that because of unsymmetric supports at the ends of bridge deck (hinge support at one end and roller support at the other), the buckling modes deviate slightly form symmetric and/or asymmetric modes.

The drag forces, lift forces, and pitching moments acting at the bridge deck at the initial undeformed deck configuration and at the flexural-torsional buckling instability are shown in **Fig.10**. It is interesting to note that each component of the displacement-dependent wind loads at instability is much larger than wind loads at initial undeformed deck configuration.

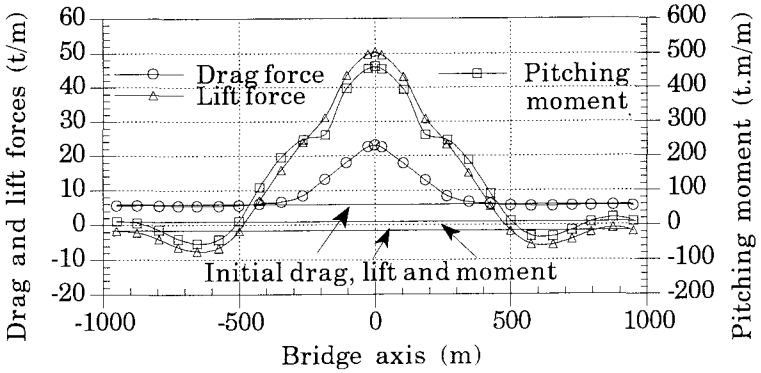

Fig.10 Three components of displacement-dependent wind load acting on the deck at nonlinear flexural-torsional buckling instability (V_{cr} = 135 m/s, $\theta_{L/2}$ = 14.2 degree)

As an evaluation of the computational efficiency, the convergence history of the critical wind velocity for nonlinear flexural-torsional buckling instability under displacement-dependent wind load is indicated in **Table 1**. The iterative procedure is initialed by using the design wind velocity as the beginning trial critical wind velocity. The true critical wind velocity is obtained after only seven outermost iteration cycles. This result shows that the present solution procedure results in good computational efficiency compared with conventional trial-and-error method.

Table 1. Convergence history of critical wind velocity under displacement-dependent wind load

Outermost iteration cycle	Est. wind velocity (m/s)	Structural stability Check	Reduced buckling load factor	Updated wind-velocity bounds		Est. wind vel. in next iteration.
				V_L	V_U	
1	57	Stable	27.33	57	299	178
2	178	Unstable	-	57	178	118
3	118	Stable	4.99	118	178	148
4	148	Unstable	-	118	148	133
5	133	Stable	2.10	133	148	140
6	140	Unstable	-	133	140	136
7	136	Unstable	-	133	136	135

5.2 Comparisons with Nonlinear Torsional Divergence

The present method for nonlinear flexural-torsional buckling instability analysis have been compared with conventional method for nonlinear torsional divergence in

Fig.8. As can be seen in the figure, the nonlinear torsional divergence analysis under only pitching moment results in greatly overestimating the critical wind velocity, compared with the nonlinear flexural-torsional buckling instability analysis under the three components of wind forces. The critical wind velocity of 135 m/s obtained from the nonlinear flexural-torsional buckling instability analysis is 31 % lower than that of 197 m/s obtained from the nonlinear torsional divergence analysis. This result shows that the nonlinear flexural-torsional buckling instability of long-span cable-stayed bridge is much more likely to occur than the torsional divergence.

5.3 Effect of Wind Angle of Incidence

The torsional and horizontal behavior at mid-point of center span obtained from the nonlinear flexural-torsional buckling instability analysis is shown for various wind angle of incidence in **Figs.11**and **12**. As can be seen in the figure, the angle of incidence has the considerable effects on both the torsional and horizontal displacement behavior of the deck as well as the critical wind velocity. The angle of incidence of positive 5 degree (head up) reduces the critical wind velocity from 135 m/s to 113 m/s.

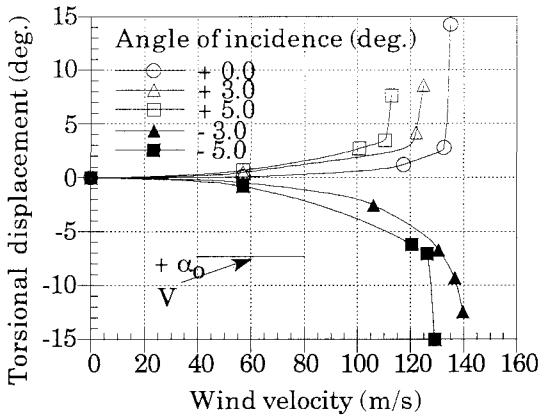

Fig.11 Torsional behavior at mid-point of center span for various wind angles of incidence

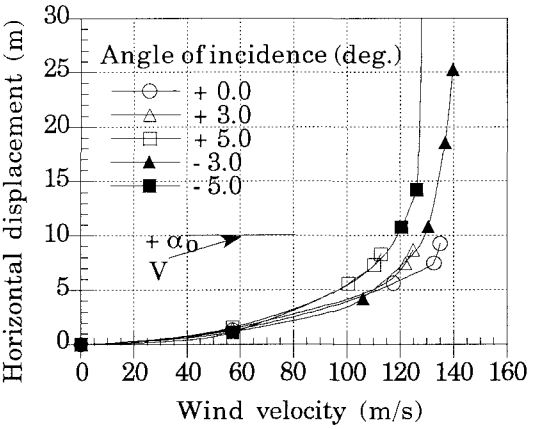

Fig.12 Horizontal displacement behavior at mid-point of center span for various wind angles of incidence

6. CONCLUSIONS

The finite-element approach to calculate the critical wind velocity for nonlinear flexural-torsional buckling instability of long-span cable-stayed bridges under the three components of displacement-dependent wind load is presented. The conclusions are summarized as follows:

(1) The incorporation of the three components of displacement-dependent wind load as well as the geometric nonlinearity in the analysis results in significant reduction of critical wind velocity, compared with the linearized buckling and torsional divergence analyses.

(2) A combination of the eigenvalue analysis and the updated wind-velocity bound algorithm for calculation of critical wind velocity under the displacement-dependent wind load results in a fast rate of convergence, compared with the trial-and-error method.

It is expected that if a cable-stayed bridge has much longer span in the future, the nonlinear flexural-torsional buckling instability under three components of displacement-dependent wind load will present a crucial mode of failure.

ACKNOWLEDMENTS

This study is financially supported by Ministry of Education, Science and Culture of Japan (Monbusho).

REFERENCES

1) Nazmy, A. S., and Abdel-Ghaffar, A. M., "Three-Dimensional Nonlinear Static Analysis of Cable-Stayed Bridges", Computers & Structures Vol. 34, No. 2, pp. 257-271, 1990
2) Argyris, J. h. et al. ,"On the Geometric Stiffness of a Beam on a Space-a Consistent Approach", Compute method in Applied Mechanics and Engineering, Vol. 20, pp. 105-131, 1979
3) Hasegawa, A. et al., "A concise and Explicit Formulation of 0ut-of-Plane of Thin-Walled Members", Structural Engineering/ Earthquake Engineering, JSCE, Vol. 2(1), pp. 57-65, 1985
4) Yang, Y. B., and McGuir, W., "Stiffness Matrix for Geometric Nonlinear Analysis", Journal of Structural Engineering, ASCE, Vol. 112(4), pp. 853-877, 1986
5) Elist, Z. M., Theory and Methods of Structural Analysis, John Wiley and Sons, New York, 1986
6) Hirai, A. et al., "Student on the Critical Wind Velocity for Suspension Bridges", International Research Seminal on Wind Effects on Buildings and Structures, Ottawa, Canada, 1967
7) Simiu, E., and Scanlan, R.H., Wind Effects on Structures, 2 nd., John Wiley and Sons, New York, 1986
8) Virlogeux, M., "Wind Design and Analysis for the Normandy Bridge", Proceeding of the First International Symposium on Aerodynamics of Large Bridges, Copenhagen, Denmark, 1992
9) Hoshino, M, and Miyata, T., "Design Trial of a Long-Span Cable-Stayed Bridge with Center Span Length of 1000 m.", Bridge and Foundation Engineering, 90-2,1990 (in Japanese)
10) Boonyapinyo, V., Nonlinear Static Instability Analysis of Long-Span Cable-Stayed Bridges under Gravity and Wind Loads, Doctoral Thesis, will be submitted to Yokohama National University, December, 1992
11) Japan Highway Public Corporation, Annual Report 1990 Technical Comm. Meikoh Cable-Stayed Bridge, Japan, 1991
12) Honshu-Shikoku Bridge Authority, Wind Resistant Design Code for Honshu-Shikoku Bridge, Japan, 1976

(Received September 21, 1992)

APPENDIX Geometrix Stiffness Matrix $[k_g^*]$: $[k_g^*]$ =

u_{xA}	u_{yA}	u_{zA}	θ_{xA}	θ_{yA}	θ_{zA}	u_{xB}	u_{yB}	u_{zB}	θ_{xB}	θ_{yB}	θ_{zB}
	$\frac{(M_{zA}+M_{zB})}{L^2}$	$\frac{-(M_{yA}+M_{yB})}{L^2}$	.	.	.	.	$\frac{-(M_{zA}+M_{zB})}{L^2}$	$\frac{(M_{yA}+M_{yB})}{L^2}$	.	.	.
	$\frac{6F_{xB}}{5L}$	.	$\frac{M_{yA}}{L}$	$\frac{M_{xB}}{L}$	$\frac{F_{xB}}{10}$	$\frac{-(M_{zA}+M_{zB})}{L^2}$	$\frac{-6F_{xB}}{5L}$	.	$\frac{M_{yB}}{L}$	$\frac{-M_{xB}}{L}$	$\frac{F_{xB}}{10}$
		$\frac{6F_{xB}}{5L}$	$\frac{M_{zA}}{L}$	$\frac{-F_{xB}}{10}$	$\frac{M_{xB}}{L}$	$\frac{(M_{yA}+M_{yB})}{L^2}$	.	$\frac{-6F_{xB}}{5L}$	$\frac{M_{zB}}{L}$	$\frac{-F_{xB}}{10}$	$\frac{-M_{xB}}{L}$
			$\frac{\overline{K}}{L}$	$\frac{(M_{zA}+M_{zB})}{6}$	$\frac{-(M_{yA}+M_{yB})}{6}$	.	$\frac{-M_{yA}}{L}$	$\frac{-M_{zA}}{L}$	$\frac{-\overline{K}}{L}$	$\frac{-(M_{zA}+M_{zB})}{6}$	$\frac{(M_{yA}+M_{yB})}{6}$
				$\frac{2F_{xB}L}{15}$	.	.	$\frac{-M_{xB}}{L}$	$\frac{F_{xB}}{10}$	$\frac{-(M_{zA}+M_{zB})}{6}$	$\frac{-F_{xB}L}{30}$	$\frac{M_{xB}}{2}$
					$\frac{2F_{xB}L}{15}$	.	$\frac{-F_{xB}}{10}$	$\frac{-M_{xB}}{L}$	$\frac{(M_{yA}+M_{yB})}{6}$	$\frac{-M_{xB}}{2}$	$\frac{-F_{xB}L}{30}$
						.	$\frac{(M_{zA}+M_{zB})}{L^2}$	$\frac{-(M_{yA}+M_{yB})}{L^2}$	.	.	$\frac{-(M_{yA}+M_{yB})}{L^2}$
							$\frac{6F_{xB}}{5L}$	.	$\frac{-M_{yB}}{L}$	$\frac{M_{xB}}{L}$	$\frac{-F_{xB}}{10}$
		Symmetric						$\frac{6F_{xB}}{5L}$	$\frac{-M_{zB}}{L}$	$\frac{F_{xB}}{10}$	$\frac{M_{xB}}{L}$
									$\frac{\overline{K}}{L}$	$\frac{(M_{zA}+M_{zB})}{6}$	$\frac{-(M_{yA}+M_{yB})}{6}$
										$\frac{2F_{xB}L}{15}$	
											$\frac{2F_{xB}L}{15}$